Published in final edited form as:

Biochim Biophys Acta Gene Regul Mech. 2023 September ; 1866(3): 194961. doi:10.1016/j.bbagrm.2023.194961.

Differences and similarities in recognition of co-factors by Taf14

Minh Chau Nguyen[a,1], **Duo Wang**[b,1], **Brianna J. Klein**[a,1], **Yong Chen**[b,*], **Tatiana G. Kutateladze**[a,*]

[a]Department of Pharmacology, University of Colorado School of Medicine, Aurora, CO 80045, USA

[b]State Key Laboratory of Molecular Biology, National Center for Protein Science Shanghai, Shanghai Institute of Biochemistry and Cell Biology, Center for Excellence in Molecular Cell Science, Chinese Academy of Sciences, Shanghai 200031, China

Abstract

Taf14 is a subunit of multiple fundamental complexes implicated in transcriptional regulation and DNA damage repair in yeast cells. Here, we investigate the association of Taf14 with the consensus sequence present in other subunits of these complexes and describe the mechanistic features that affect this association. We demonstrate that the precise molecular mechanisms and biological outcomes underlying the Taf14 interactions depend on the accessibility of binding interfaces, the ability to recognize other ligands, and a degree of sensitivity to temperature and chemical and osmotic stresses. Our findings aid in a better understanding of how the distribution of Taf14 among the complexes is mediated.

Keywords

Taf14; ET domain; YEATS; Tfg1; Ino80; Snf5; Taf2; Sth1; Mechanism

1. Introduction

Transcription initiation factor subunit 14 (Taf14) is a multifunctional yeast protein identified in a diverse set of chromatin associating complexes implicated in transcriptional regulation, DNA damage repair, chromosome maintenance, and cell cycle progression (Fig. 1a). Taf14 is an integral component of the general transcription factor (TF) complex TFIID, which binds to gene promoters and plays a critical role in the assembly of the preinitiation complex (PIC), and the TFIIF complex, which recruits RNA polymerase II (RNA Pol II) to PIC [1–

*Corresponding authors. yongchen@sibcb.ac.cn (Y. Chen), tatiana.kutateladze@cuanschutz.edu (T.G. Kutateladze).

[1]Equal contribution.

Supplementary data to this article can be found online at https://doi.org/10.1016/j.bbagrm.2023.194961.

CRediT authorship contribution statement

M.C.N., D.W. and B.J.K. performed experiments and together with Y. C. and T.G.K. analyzed the data. T.G.K. wrote the manuscript with input from all authors.

Declaration of competing interest

The authors declare the following financial interests/personal reationships which may be considered as potential competing interests: Tatiana G Kutateladze reports financial support was provided by National Institutes of Health. Tatiana G Kutateladze reports a relationship with NIH that includes: funding grants.

5]. Taf14 is also present in the histone acetyltransferase complex NuA3 that acetylates lysine 14 of histone H3 and facilitates transcription elongation [6], and in the ATP-dependent chromatin-remodeling complexes INO80, SWI/SNF and RSC [3,7,8]. In addition, Taf14 is functionally linked to the transcript elongation factor TFIIS, which promotes elongation by RNA Pol II [9], and to the mediator complex [10]. Taf14 is required for the mitotic cell cycle progression, and Taf14 depleted cells are characterized by cytoskeletal and morphological defects, diminished transcription *in vivo*, and are thermosensitive [2,11].

Taf14 contains two folded domains, the YEATS (Yaf9, ENL, AF9, Taf14, Sas5) domain and the ET (extra-terminal) domain, coupled *via* a short linker (Fig. 1b). The YEATS domain of Taf14 is a well-established reader of acylated lysine 9 of histone H3 (H3K9acyl), and this function is essential in transcriptional regulation and DNA-damage response [12–15]. The unstructured linker is implicated in DNA binding, and this activity depends on dynamic equilibrium between autoinhibited and open states of Taf14 [16]. The ET domain has been shown to recognize the 'hxh + h' motif [where h is a hydrophobic residue, + is a positively charged residue, and x is any residue] and named EBM (ET binding motif). EBM is present in co-factors, such as Sth1, a subunit of the RSC complex, and Taf2, a subunit of TFIID [16,17]. Interestingly, the ET domain of Taf14 undergoes liquid-liquid phase separation (LLPS) with the cofactor binding stimulating LLPS [17]. The LLPS capability was proposed to concentrate the Taf14-containing complexes at specific chromatin loci and drive efficient gene expression [17]. Because Taf14 is present in multiple and distinctly different yeast complexes, its precise biological role within each complex remains difficult to define.

In this study, we use structural, biochemical and mutagenesis tools to identify mechanistic features that affect the Taf14 engagement with co-factors from different complexes. Our genetic analysis using mutated co-factors provides an approach to disrupt the Taf14 association with individual co-factors and therefore dissect the role of Taf14 independently in each complex.

2. Results and discussion

2.1. EBMs occupy a conserved binding site of Taf14$_{ET}$

Structural analysis of the Taf14 ET domain (Taf14$_{ET}$) in complex with Sth1 peptide or Taf2 peptide shows that the peptides are bound in a cleft formed by α1 helix and β-sheet of the protein [16,17] (Fig. 1c). Both Sth1 and Taf2 contain the hxh + h sequence, or EBM, which is also present in Tfg1 (Tfg1$_{EBM}$), a catalytic subunit of TFIIF, in Ino80 (Ino80$_{EBM}$), a catalytic subunit of the INO80 complex, and in Snf5 (Snf5$_{EBM}$), a catalytic subunit of the SWI/SNF complex (Fig. 1d). We used NMR spectroscopy to assess whether the EBM recognition mode is conserved for other ligands of Taf14$_{ET}$. We generated uniformly ^{15}N-labeled Taf14$_{ET}$ and recorded its ^{1}H,^{15}N heteronuclear single quantum coherence (HSQC) spectra as unlabeled Tfg1$_{EBM}$ (aa 614–625), Ino80$_{EBM}$ (aa 368–379) and Snf5$_{EBM}$ (aa 782–793) peptides were gradually added to the protein samples (Fig. 1e). Large chemical shift perturbations (CSPs) induced by either Tfg1$_{EBM}$, Ino80$_{EBM}$ or Snf5$_{EBM}$ in Taf14$_{ET}$ indicated formation of the complexes (Fig. 1e). A number of amide resonances of Taf14$_{ET}$ that were observed in the apo-state disappeared upon addition of the peptides, and another set of crosspeaks corresponding to the EBM-bound state of Taf14$_{ET}$ appeared. The slow

and slow-to-intermediate exchange regime on the NMR timescale suggested tight binding, and an overall similar pattern of CSPs induced by each peptide, as well as $Taf2_{EBM}$ [16], indicated that these ligands are bound in the same binding site of $Taf14_{ET}$.

2.2. Contribution of hydrophobic and ionic contacts

The structure of the $Taf14_{ET}$-$Taf2_{EBM}$ complex reveals that $Taf2_{EBM}$ forms the third anti-parallel β-strand, pairing with the second β-strand of $Taf14_{ET}$, and that the complex is stabilized through extensive intermolecular contacts [16] (Fig. 1f). These include the backbone-backbone hydrogen bonds, hydrophobic contacts involving the side chains of V1397 and I1399 of $Taf2_{EBM}$ that are buried in the hydrophobic cleft of $Taf14_{ET}$, as well as electrostatic interactions involving R1400 and K1398 of $Taf2_{EBM}$. AlphaFold derived models of full length Tfg1, Ino80 and Snf5 show that $Tfg1_{EBM}$, $Ino80_{EBM}$ and $Snf5_{EBM}$ adopt an extended conformation even in the apo-states of these proteins (Suppl. Fig. 1). Notably, $Snf5_{EBM}$ and $Tfg1_{EBM}$ superimpose with $Taf2_{EBM}$ or $Sth1_{EBM}$ bound to $Taf14_{ET}$ with an rmsd (root-mean-square deviation) of 0.9 Å and 2.8 Å, respectively (Fig. 1f). We also found that hydrophobic contacts are required for binding of these ligands, as a single point mutation of either I618 or L620 in $Tfg1_{EBM}$ to an aspartate abolished the inter-action with $Taf14_{ET}$ (Fig. 1g).

To delineate the contribution of hydrophobic and ionic contacts, we tested formation of the $Taf14_{ET}$-$Sth1_{EBM}$ complex in variable salt concentrations using pull-down assays. GST-$Taf14_{ET}$ and Sumo-$Sth1_{EBM}$ were incubated with glutathione Sepharose beads at 4 °C or room temperature (RT) and Sumo-$Sth1_{EBM}$ bound $Taf14_{ET}$ was detected by electrophoresis (Fig. 2a, b). As shown in Fig. 2a, an increase in concentration of NaCl from 300 mM to 800 mM resulted in a reduced binding of $Sth1_{EBM}$, indicating that electrostatic interactions are essential for the formation of the tight complex which can be regulated by osmotic pressure (Fig. 2c). Still, the binding was not completely abolished even at a salt concentration of 1 M, indicating that hydrophobic contacts are the driving force of this interaction (Fig. 2b).

Interestingly, we found that in contrast to the binding of $Ino80_{EBM}$ or $Snf5_{EBM}$ (data not shown), the interaction between $Taf14_{ET}$ and $Sth1_{EBM}$ is temperature sensitive. GST-$Taf14_{ET}$ pulled down more $Sth1_{EBM}$ with the increase of the reaction temperature (Fig. 2a, b). Together, these data suggest that the degree of temperature and osmotic adaptation could mediate the ability of Taf14 to form complexes to ensure the optimal growth and proliferation of the mesophilic yeast.

2.3. Diverse mechanisms of the Taf14 complex formation

We have previously shown that both domains of Taf14, $Taf14_{ET}$ and $Taf14_{YEATS}$, are capable of binding to $Taf2_{EBM}$ and proposed a model in which $Taf2_{EBM}$ is sandwiched between $Taf14_{ET}$ and $Taf14_{YEATS}$ [16]. Upon $Taf2_{EBM}$ binding, a contiguous twisted β-sheet encompassing both domains of Taf14 could be created to release the linker region of Taf14 for binding to DNA (Fig. 3a, b). As shown in Fig. 3c, full length $Taf14_{FL}$ maintained the ability to bind EBM peptides in NMR titration experiments. Much like $Taf2_{EBM}$, $Ino80_{EBM}$, $Snf5_{EBM}$, and $Tfg1_{EBM}$ induced CSPs in ^{15}N-labeled $Taf14_{FL}$ (Fig. 3c). However, CSPs in ^{1}H,^{15}N HSQC spectra of the isolated ^{15}N-labeled $Taf14_{YEATS}$ were

caused only by $Taf2_{EBM}$ (Fig. 3d). The inability of $Ino80_{EBM}$, $Snf5_{EBM}$, and $Tfg1_{EBM}$ to induce significant resonance changes indicated that in contrast to $Taf2_{EBM}$, these EMBs do not interact with $Taf14_{YEATS}$ and pointed to the unique binding mechanism that differentiates the Taf14-Taf2 complex formation.

The dual domain engagement with $Taf2_{EBM}$ in $Taf14_{FL}$ led to a ~ two-fold tighter binding compared to the interaction of an isolated $Taf14_{ET}$ with $Taf2_{EBM}$ [16] (Fig. 4a). However, the full-length Taf14 protein has been shown to exist in a dynamic equilibrium between the autoinhibited state, in which $Taf14_{ET}$ associates with the linker and therefore is not easily accessible, and the open state, in which $Taf14_{ET}$ is more freely available (Fig. 4b). To test whether the $Taf14_{FL}$ autoinhibition affects interactions with $Ino80_{EBM}$, $Snf5_{EBM}$, $Sth1_{EBM}$ and $Tfg1_{EBM}$, we measured binding affinities by microscale thermophoresis (MST) (Fig. 4a, c and Suppl. Fig. 2). The measurements showed that compared to the isolated $Taf14_{ET}$ [17], $Taf14_{FL}$ associated five-fold weaker with $Ino80_{EBM}$ and seven-fold weaker with $Snf5_{EBM}$, but its binding to $Sth1_{EBM}$ and $Tfg1_{EBM}$ was unaffected. Much like the isolated domain, the full length protein had highest binding affinity toward $Sth1_{EBM}$ and $Ino80_{EBM}$ (dissociation constants (K_ds) of 0.07 μM and 1.2 μM, respectively) (Fig. 4a).

Another aspect of the Taf14-EBM complex formation that needs to be taken into account is the accessibility of EBM sequences in full length proteins which can fine tune the assembly of the complexes. Even though $Taf2_{EBM}$ is located in the C-terminal tail of the protein, the AlphaFold model of $Taf2_{FL}$ suggests that this region is involved in intramolecular contacts that may impede binding to Taf14 (Fig. 4d). Similarly, it is unclear how accessible $Ino80_{EBM}$, $Snf5_{EBM}$, $Sth1_{EBM}$ and $Tfg1_{EBM}$ are in the context of full length Ino80, Snf5, Sth1 and Tfg1 proteins (Fig. 4d) and whether this accessibility is regulated by interactions with other ligands and/or conformational changes. Clearly, the binding capability of Taf14 have to be re-examined in the context of full length EBM-containing proteins.

2.4. EBM recognition is linked to distinct biological outcomes

To explore the ways to independently characterize the functional significance of EBM recognition by Taf14, we investigated the phenotypes of yeast strains in which binding of Snf5 and separately binding of Sth1 to Taf14 was disrupted. We generated yeast strains harboring L1204A/V1206A/I1208A/L1210A mutant of Sth1 ($sth1^{M4}$) and L785A/L787A/I789A/L791A mutant of Snf5 ($snf5^{M4}$) that are impaired in binding to $Taf14_{ET}$ [17]. The plasmids carrying *SNF5* or $snf5^{M4}$ were transformed into a *snf5Δ* strain. As *sth1* is an essential gene, we transformed the diploid strain BY4743 with plasmids carrying either wt *STH1* or $sth1^{M4}$ and isolated spore clones carrying *STH1* or $sth1^{M4}$ plasmids. The $sth1^{M4}$ strain with the Taf14-binding deficient mutant of Sth1 displayed heat-sensitivity and failed to grow at 34 °C or 37 °C (Fig. 5a). In contrast, the $snf5^{M4}$ strain with the Taf14-binding deficient mutant of Snf5 grew faster than wt at all temperatures tested (Fig. 5b). Collectively, these results, together with the findings that the deletion of $Taf2_{EBM}$ leads to a mild slow growth phenotype while preventing the stable association of Taf14 with TFIID [18], pointed to distinct roles of the EBM recognition which can be examined through impairing EBMs. Our data, for example, suggested that, unlike binding of Sth1, binding of Snf5 to Taf14 might be important for repressive action of the SWI/SNF complex. However, we cannot

exclude the possibility that once the SWI/SNF complex is depleted of Taf14 due to defective $Snf5_{EBM}$, more Taf14 is available to other complexes, and such a redistribution of Taf14 could also perturb functions of these complexes.

Comparison of the phenotypes of wt *STH1* and $sth1^{M4}$ yeast strains and wt *SNF5* and $snf5^{M4}$ yeast strains in response to DNA-damage agents, including methyl methanesulfonate (MMS), phleomycin (Phle), and hydroxyurea (HU) further confirmed the effectiveness of this approach in studying biological effects associated with the recognition of diverse EBM ligands. The $sth1^{M4}$ yeast strain showed slight growth defects compared to the wt *STH1* yeast strain (Fig. 5c), but the $snf5^{M4}$ yeast strain grew much better than wt *SNF5* strain in the presence of these drugs (Fig. 5d).

2.5. Concluding remarks

The findings that $Taf14_{ET}$ associates with several essential co-factors through recognizing their EBM sequences raises the question as to what are the mechanisms that control the distribution of Taf14 among the co-factor-containing complexes in yeast cells. In this study, we show that while isolated EBM peptides tested are readily recognized by $Taf14_{ET}$, the molecular mechanisms and biological outcomes of the full length Taf14 interactions differ and depend on a variety of factors, including the ability of EBMs to alleviate the Taf14 autoinhibitory state and interact with other ligands. In addition, the Taf14-containing complexes can be characterized by a different degree sensitivity to temperature, nutrient, chemical and osmotic stresses and likely depend on the accessibility of the EBM sequences in the context of full length ligand proteins. The latter could have a profound impact on Taf14 incorporation into the complexes, necessitating thorough investigation of the interactions between full length binding partners.

We further demonstrate the feasibility of characterization of the role of Taf14 in specific complexes through a design of EBM-impaired co-factors. This approach expands our previous work showing that the disruption of Taf14-EBM interaction within the RSC complex results in yeast cells incapable of growing at high temperature and alters the transcription of genes involved in heat-response and catabolic metabolism [17]. Although some Taf14-mediated interactions have been characterized at the atomic resolution level [12,14–17], to better understand the differences in binding co-factors, structures of other complexes need to be elucidated. Additionally, cryo-EM studies could provide a comprehensive view of the entire complexes and may reveal additional contacts of Taf14 with other subunits to fine tune the complex assemblies and functions.

3. Methods

3.1. Protein purification

The *S. cerevisiae* GST- and His-tagged $Taf14_{FL}$ (aa 1–244), $Taf14_{YEATS}$ (aa 1–137), and $Taf14_{ET}$ (aa 168–243 and aa 162–243 K163N/R164Q/K166N) were expressed in *Escherichia coli* Rosetta-2 (DE3) pLysS cells grown in either Terrific Broth, Luria Broth or minimal media supplemented with $^{15}NH_4Cl$ (Sigma). Protein production was induced with 0.3 mM IPTG for 18 h at 16 °C. Bacteria were harvested by centrifugation and

lysed by sonication. GST-fusion proteins were purified on glutathione agarose 4B beads (Thermo Fisher Sci). The GST-tag was cleaved with either PreScission or tobacco etch virus (TEV) protease. His-fusion proteins were purified on a Ni-NTA resin (ThermoFisher) and eluted with a gradient of imidazole. The His-tag was cleaved with TEV protease and removed by dialysis. Unlabeled proteins were further purified by column chromatography and concentrated in Millipore concentrators (Millipore). For pull-down assays, $Sth1_{EBM}$-containing fragment (aa 1183–1240) was expressed as a 6xHis-Sumo-tagged protein and purified as above.

3.2. NMR experiments

Nuclear magnetic resonance (NMR) experiments were performed at 298 K on Varian INOVA 900 MHz and 600 MHz spectrometers equipped with cryogenic probes. The NMR samples contained 0.1–0.3 mM uniformly ^{15}N-labeled $Taf14_{FL}$, $Taf14_{YEATS}$, or $Taf14_{ET}$ in 50 mM Tris-HCl pH 6.6–7.5, 150 mM NaCl, 0–5 mM DTT or 0.2 mM TCEP or in PBS pH 6.6–7.5, 0–5 mM DTT and 8–10 % D_2O. Binding was characterized by monitoring chemical shift changes in ^{1}H,^{15}N HSQC spectra of the proteins induced by the addition of $Tfg1_{EBM}$ (aa 614–625), $Ino80_{EBM}$ (aa 368–379), $Snf5_{EBM}$ (aa 782–793) and $Taf2_{EBM}$ (aa 1392–1402) peptides (synthesized by Synpeptide). NMR data were processed and analyzed as described [19].

3.3. GST pull-down assays

For pull-down assays, 50 μg of GST-tagged $Taf14_{ET}$ and 50 μg Sumo-$Sth1_{EBM}$ were mixed with 10 μL of glutathione Sepharose 4B beads in 100 μL of binding buffer (25 mM Tris-HCl, pH 8.0, 300 mM/ 500 mM/ 800 mM /1 M NaCl, and 2 mM DTT). 10 μL reaction mixtures were taken out as input controls. After incubation at the indicated temperature for 3 h, the beads were washed four times with 500 μL of the binding buffer. The bound samples were eluted with 25 μL elution buffer (15 mM reduced glutathione, 25 mM Tris-HCl, pH 8.0, 300 mM/500 mM/800 mM/1 M NaCl, and 2 mM DTT). The input and eluted samples were analyzed by SDS-PAGE.

3.4. MST

Microscale thermophoresis (MST) experiments were performed using a Monolith NT.115 instrument (NanoTemper). All experiments were performed using SEC purified His-$Taf14_{FL}$ protein in a buffer containing 20 mM Tris-HCl pH 7.5, 150 mM NaCl and 0–0.2 mM TCEP. His-$Taf14_{FL}$ was labeled using a His-Tag Labeling Kit RED-tris-NTA (2nd Generation, Nanotemper), and concentration of each labeled protein was kept at 10 nM. Dissociation constants were determined using a direct binding assay in which increasing amounts of unlabeled binding partner ($Tfg1_{EBM}$, $Snf5_{EBM}$, $Sth1_{EBM}$ or $Ino80_{EBM}$ peptides) were added stepwise. The measurements were performed at 40 % LED and medium MST power with 3 s steady state, up to 20 s laser on time and 1 s off time. The K_d values were calculated using MO Affinity Analysis software (NanoTemper) ($n = 3$; 2 for Snf5). Plots were generated in GraphPad PRISM.

3.5. Stress resistance assay and growth assay

Yeast strains were cultured in YC medium at 30 °C and suspended in sterile water at a final concentration of OD_{600} ~ 0.3. Five-fold serial dilutions were plated onto YC medium containing the different concentrations of HU, MMS, and Phle. Plates were incubated at different temperatures for 2–3 days and photographed. Each assay was repeated three times, and all showed consistent results, therefore one representative result is shown.

Supplementary Material

Refer to Web version on PubMed Central for supplementary material.

Acknowledgements

We thank R. Singh for help with experiments. This work was supported in part by grants from the NIH: GM125195 and GM135671 to T. G.K., the Shanghai Pilot Program for Basic Research from Chinese Academy of Science (JCYJ-SHFY-2022-008) to Y.C., and the Shanghai Sailing Program (22YF1453800) and China Postdoctoral Science Foundation (2022M710145) to D.W.

Data availability

Data will be made available on request.

References

[1]. Poon D, Bai Y, Campbell AM, Bjorklund S, Kim YJ, Zhou S, Kornberg RD, Weil PA, Identification and characterization of a TFIID-like multiprotein complex from Saccharomyces cerevisiae, Proc. Natl. Acad. Sci. U. S. A 92 (18) (1995) 8224–8228. [PubMed: 7667272]

[2]. Henry NL, Campbell AM, Feaver WJ, Poon D, Weil PA, Kornberg RD, TFIIF-TAF-RNA polymerase II connection, Genes Dev 8 (23) (1994) 2868–2878. [PubMed: 7995524]

[3]. Kabani M, Michot K, Boschiero C, Werner M, Anc1 interacts with the catalytic subunits of the general transcription factors TFIID and TFIIF, the chromatin remodeling complexes RSC and INO80, and the histone acetyltransferase complex NuA3, Biochem. Biophys. Res. Commun 332 (2) (2005) 398–403. [PubMed: 15896708]

[4]. Robinson PJ, Trnka MJ, Bushnell DA, Davis RE, Mattei PJ, Burlingame AL, Kornberg RD, Structure of a complete mediator-RNA polymerase II pre-initiation complex, Cell 166 (6) (2016), 1411–1422 e16. [PubMed: 27610567]

[5]. Kolesnikova O, Ben-Shem A, Luo J, Ranish J, Schultz P, Papai G, Molecular structure of promoter-bound yeast TFIID, Nat. Commun 9 (1) (2018) 4666. [PubMed: 30405110]

[6]. John S, Howe L, Tafrov ST, Grant PA, Sternglanz R, Workman JL, The something about silencing protein, Sas3, is the catalytic subunit of NuA3, a yTAF (II)30-containing HAT complex that interacts with the Spt16 subunit of the yeast CP (Cdc68/Pob3)-FACT complex, Genes Dev 14 (10) (2000) 1196–1208. [PubMed: 10817755]

[7]. Shen X, Preparation and analysis of the INO80 complex, Methods Enzymol 377 (2004) 401–412. [PubMed: 14979041]

[8]. Cairns BR, Henry NL, Kornberg RD, TFG/TAF30/ANC1, a component of the yeast SWI/SNF complex that is similar to the leukemogenic proteins ENL and AF-9, Mol. Cell. Biol 16 (7) (1996) 3308–3316. [PubMed: 8668146]

[9]. Fish RN, Ammerman ML, Davie JK, Lu BF, Pham C, Howe L, Ponticelli AS, Kane CM, Genetic interactions between TFIIF and TFIIS, Genetics 173 (4) (2006) 1871–1884. [PubMed: 16648643]

[10]. Kim YJ, Bjorklund S, Li Y, Sayre MH, Kornberg RD, A multiprotein mediator of transcriptional activation and its interaction with the C-terminal repeat domain of RNA polymerase II, Cell 77 (4) (1994) 599–608. [PubMed: 8187178]

[11]. Dahan O, Kupiec M, The Saccharomyces cerevisiae gene CDC40/PRP17 controls cell cycle progression through splicing of the ANC1 gene, Nucleic Acids Res 32 (8) (2004) 2529–2540. [PubMed: 15133121]

[12]. Shanle EK, Andrews FH, Meriesh H, McDaniel SL, Dronamraju R, DiFiore JV, Jha D, Wozniak GG, Bridgers JB, Kerschner JL, Krajewski K, Martin GM, Morrison AJ, Kutateladze TG, Strahl BD, Association of Taf14 with acetylated histone H3 directs gene transcription and the DNA damage response, Genes Dev 29 (17) (2015) 1795–1800. [PubMed: 26341557]

[13]. Andrews FH, Shanle EK, Strahl BD, Kutateladze TG, The essential role of acetyllysine binding by the YEATS domain in transcriptional regulation, Transcription 7 (1) (2016) 14–20. [PubMed: 26934307]

[14]. Andrews FH, Shinsky SA, Shanle EK, Bridgers JB, Gest A, Tsun IK, Krajewski K, Shi XB, Strahl BD, Kutateladze TG, The Taf14 YEATS domain is a reader of histone crotonylation, Nat. Chem. Biol 12 (6) (2016) 396–398. [PubMed: 27089029]

[15]. Klein BJ, Ahmad S, Vann KR, Andrews FH, Mayo ZA, Bourriquen G, Bridgers JB, Zhang J, Strahl BD, Cote J, Kutateladze TG, Yaf9 subunit of the NuA4 and SWR1 complexes targets histone H3K27ac through its YEATS domain, Nucleic Acids Res 46 (1) (2018) 421–430. [PubMed: 29145630]

[16]. Klein BJ, Feigerle JT, Zhang J, Ebmeier CC, Fan L, Singh RK, Wang WW, Schmitt LR, Lee T, Hansen KC, Liu WR, Wang YX, Strahl BD, Anthony Weil P, Kutateladze TG, Taf2 mediates DNA binding of Taf14, Nat. Commun 13 (1) (2022) 3177. [PubMed: 35676274]

[17]. Chen G, Wang D, Wu B, Yan F, Xue H, Wang Q, Quan S, Chen Y, Taf14 recognizes a common motif in transcriptional machineries and facilitates their clustering by phase separation, Nat. Commun 11 (1) (2020) 4206. [PubMed: 32826896]

[18]. Feigerle JT, Weil PA, The C terminus of the RNA polymerase II transcription factor IID (TFIID) subunit Taf2 mediates stable association of subunit Taf14 into the yeast TFIID complex, J. Biol. Chem 291 (43) (2016) 22721–22740. [PubMed: 27587401]

[19]. Gatchalian J, Futterer A, Rothbart SB, Tong Q, Rincon-Arano H, Sanchez de Diego A, Groudine M, Strahl BD, Martinez AC, van Wely KH, Kutateladze TG, Dido3 PHD modulates cell differentiation and division, Cell Rep 4 (1) (2013) 148–158. [PubMed: 23831028]

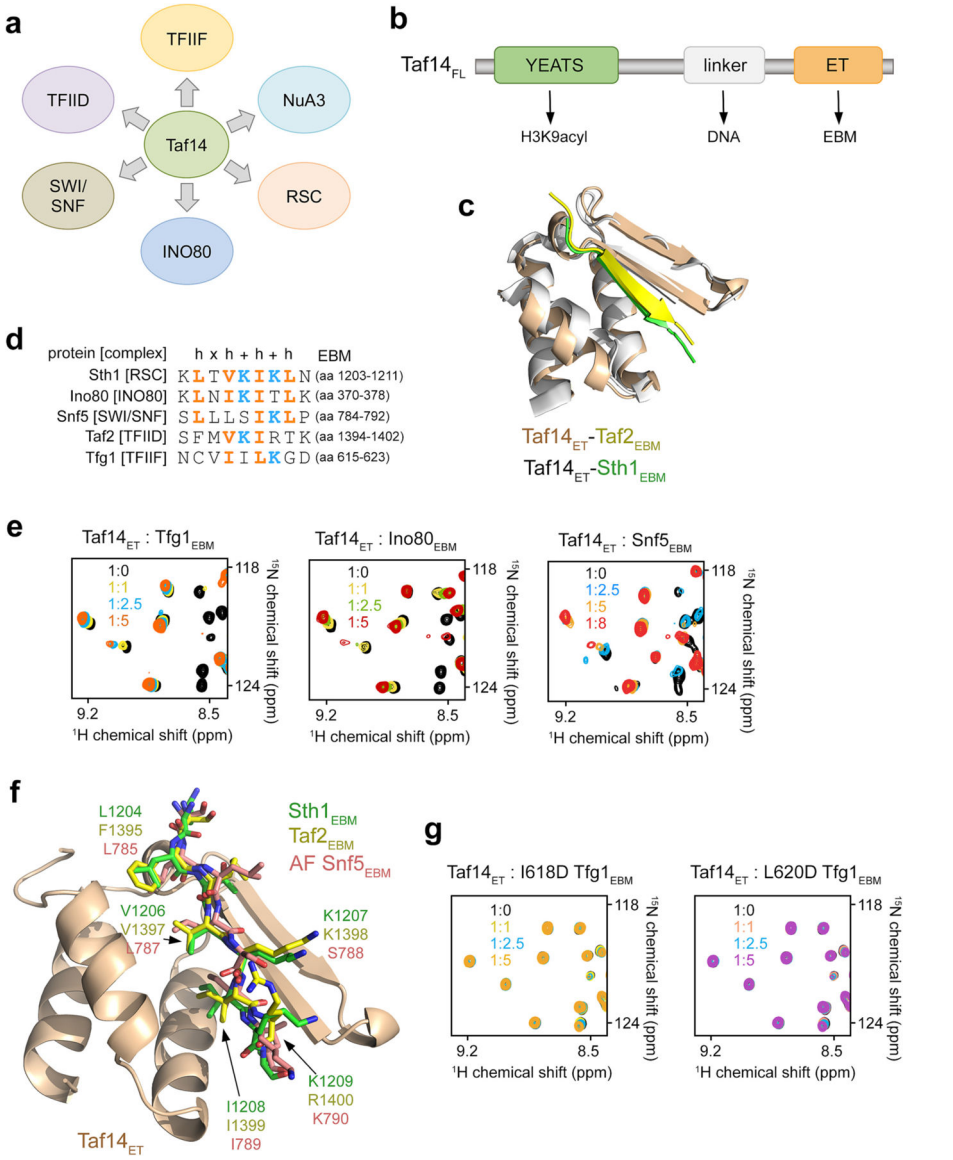

Fig. 1.

EBM binding site of $Taf14_{ET}$. (a) Taf14 is a component of a diverse set of yeast complexes. (b) Domain architecture of full length Taf14 ($Taf14_{FL}$). (c) Structural overlay of $Taf14_{ET}$ (grey) in complex with $Sth1_{EBM}$ (green) (PDB 6LQZ) and $Taf14_{ET}$ (wheat) in complex with $Taf2_{EBM}$ (yellow) (PDB 7UHE). (d) Alignment of the EBM (ET domain binding motif) sequences from Ino80, Taf2, Tfg1, Snf5 and Sth1 proteins. In the consensus sequence, h is a hydrophobic residue, + is a positively charged residue, and x is any residue. Conserved hydrophobic and lysine residues are orange and blue, respectively. (e) Superimposed $^{1}H,^{15}N$ HSQC spectra of $Taf14_{ET}$ recorded in the presence of increasing amounts of $Tfg1_{EBM}$, $Ino80_{EBM}$ and $Snf5_{EBM}$. The spectra are colour coded according to the protein:peptide molar ratio. (f) Structural overlay of $Sth1_{EBM}$ (green) from the $Taf14_{ET}$-$Sth1_{EBM}$ complex, $Taf2_{EBM}$ (dark yellow) from the $Taf14_{ET}$-$Taf2_{EBM}$ complex, and $Snf5_{EBM}$ (salmon) from $Snf5_{FL}$ generated by AlphaFold. $Taf14_{ET}$ (wheat) only from the $Taf14_{ET}$-$Taf2_{EBM}$ complex

is shown as a ribbon for clarity. Residues of EBM peptides are shown as sticks and labeled. (g) Superimposed $^{1}H,^{15}N$ HSQC spectra of $Taf14_{ET}$ recorded in the presence of increasing amounts of the indicated mutants of $Tfg1_{EBM}$. The spectra are colour coded according to the protein:peptide molar ratio.

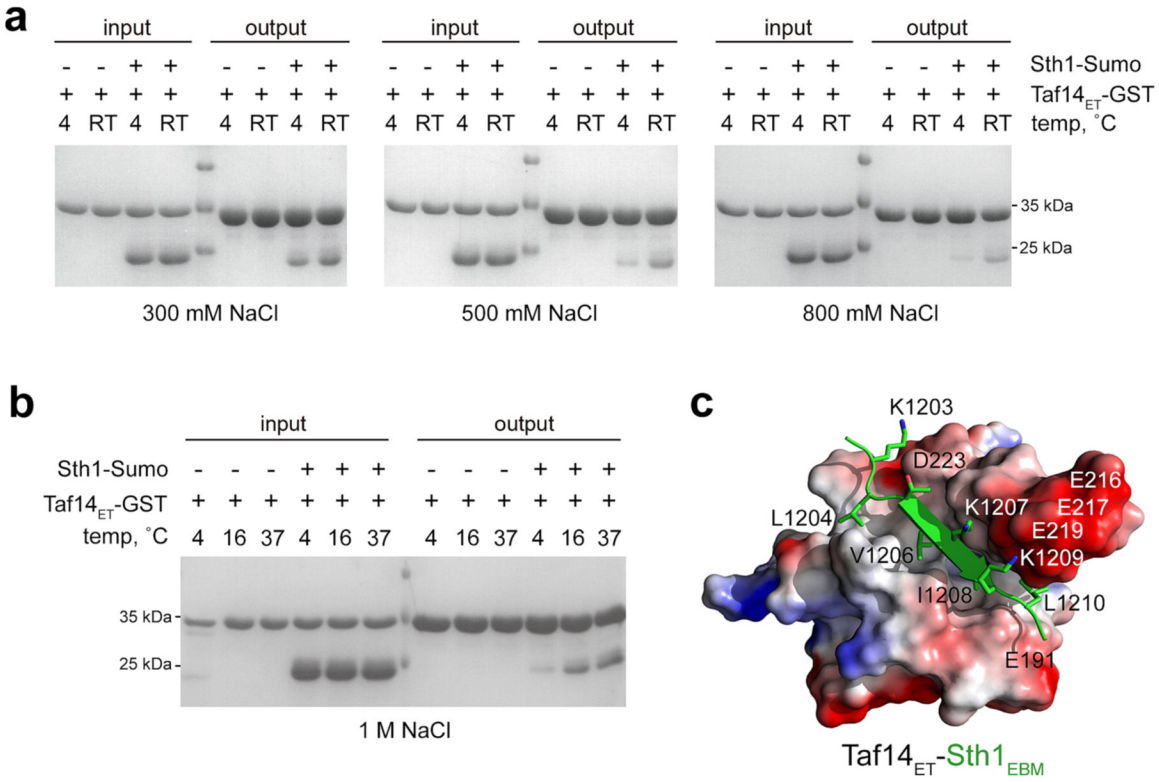

Fig. 2.

Effects of hydrophobic and ionic contacts. (a, b) SDS-PAGE gels showing binding of SUMO-Sth1$_{EBM}$ to GST-Taf14$_{ET}$ on glutathione Sepharose 4B beads at indicated temperature and NaCl concentrations. (c) The structural model of the Taf14$_{ET}$-Sth1$_{EBM}$ complex. Taf14$_{ET}$ is shown as a surface model colored according to its electrostatic potential (positive potential is blue and negative potential is red). Residues of the Sth1$_{EBM}$ peptide are shown as green sticks.

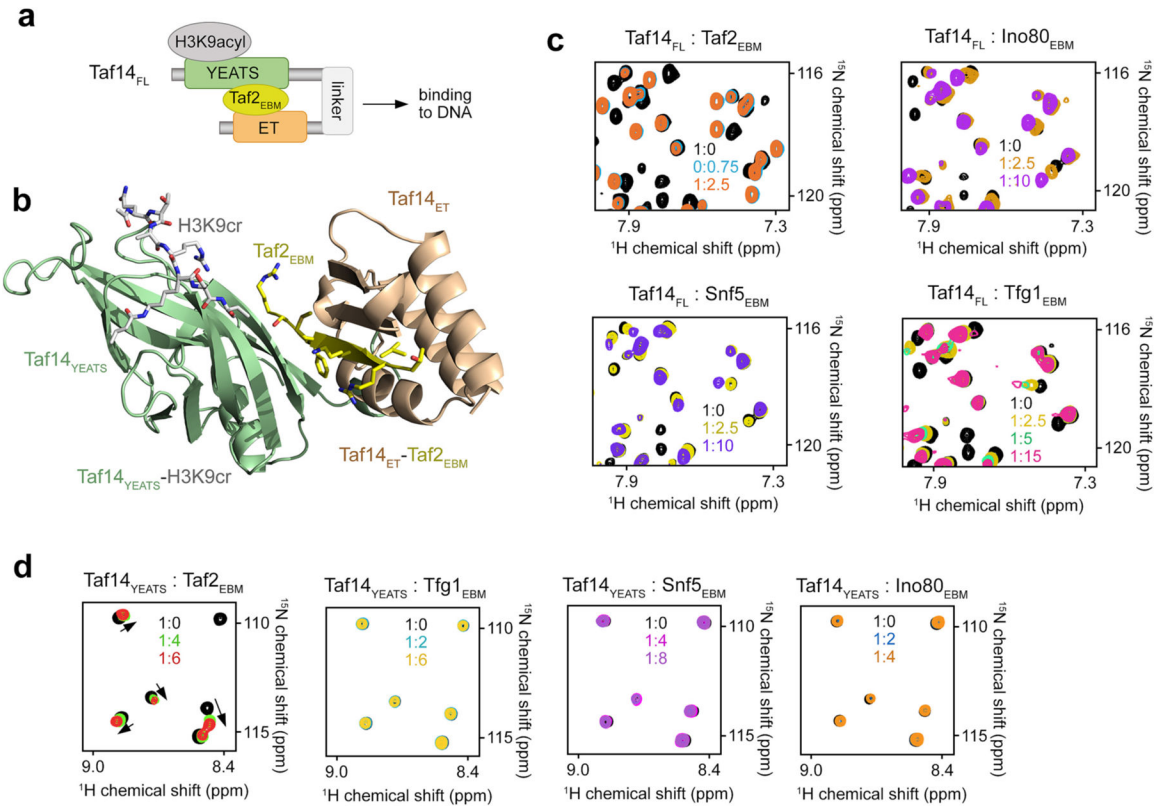

Fig. 3.

Unique mechanisms of the Taf14 complex formation. (a) Schematic of $Taf14_{FL}$ in complex with H3K9acyl and $Taf2_{EBM}$. (b) Overlay of the crystal structures of the $Taf14_{YEATS}$:H3K9cr complex (light green:grey), $Taf14_{ET}$:$Taf2_{EBM}$ complex (wheat:yellow), and the cryo-EM structure of $Taf14_{FL}$ in the RNA Pol II TFIIF complex (5SVA, not shown) [4]. (c, d) Superimposed ^{1}H,^{15}N HSQC spectra of $Taf14_{FL}$ (c) or $Taf14_{YEATS}$ (d) recorded in the presence of increasing amounts of the indicated EBMs. $Taf2_{EBM}$ data are from [16]. The spectra are colour coded according to the protein:peptide molar ratio.

a

protein	ligand	K_d (μM)
$Taf14_{FL}$	$Taf2_{EBM}$	0.7 ± 0.1
$Taf14_{ET}$	$Taf2_{EBM}$	1.6 ± 0.4
$Taf14_{FL}$	$Ino80_{EBM}$	1.2 ± 0.2
$Taf14_{FL}$	$Snf5_{EBM}$	18 ± 1
$Taf14_{FL}$	$Sth1_{EBM}$	0.07 ± 0.01
$Taf14_{FL}$	$Tfg1_{EBM}$	16 ± 2

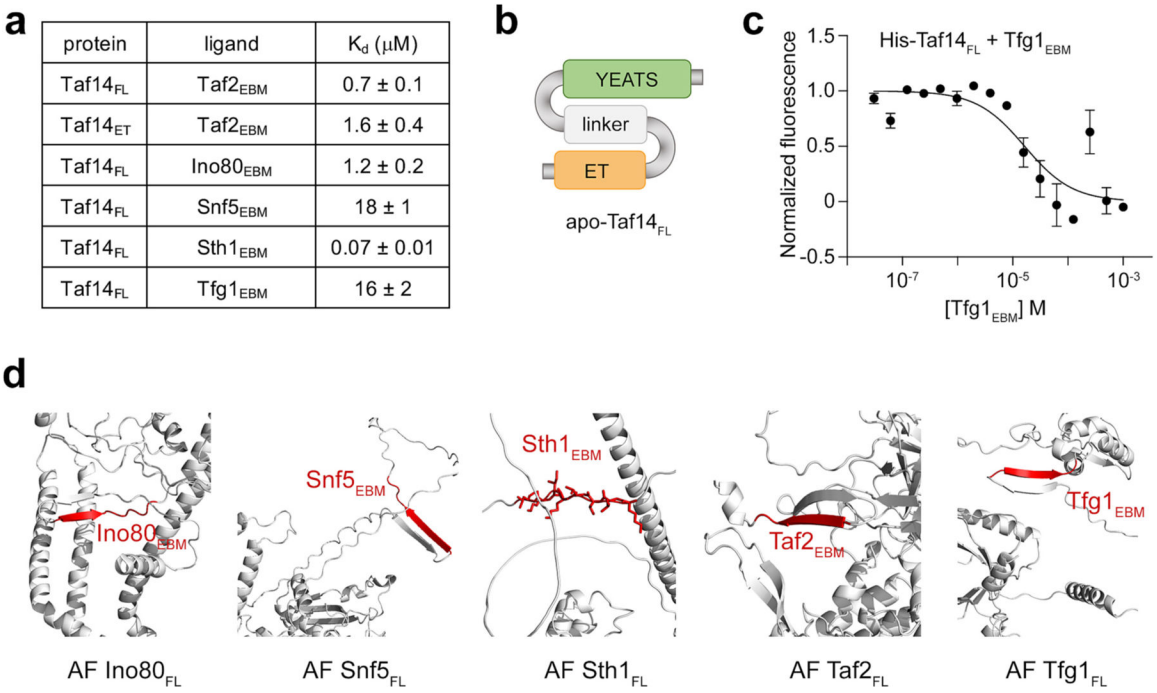

Fig. 4.

Full length $Taf14_{FL}$ binds EBM. (a) Binding affinities to indicated EBMs measured by MST. K_d values represent average of three independent measurements ± SEM (two for Snf5). $Taf2_{EBM}$ data are from [16]. (b) A model of the autoinhibited apo-state of $Taf14_{FL}$. (c) MST binding curve for the interaction of $Taf14_{FL}$ with $Tfg1_{EBM}$. The K_d value represents average of three independent measurements ± SEM, and error bars represent SEM for each point. $n = 3$ (d) AlphaFold generated models of the structures of the EBM-containing proteins in apo-states. The EBM sequence is red.

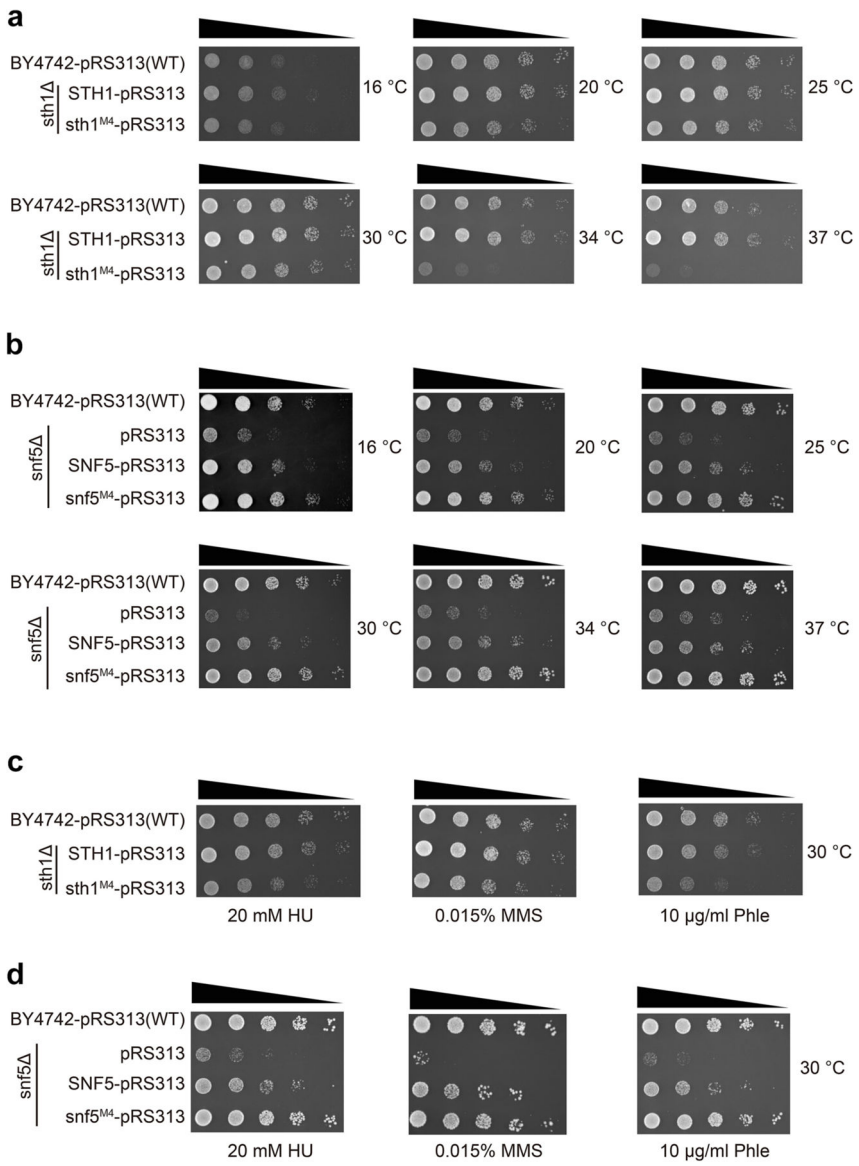

Fig. 5.

Genetic analyses of the Taf14-Sth1 and Taf14-Snf5 interactions. (a) Spotting assays with *sth1Δ* strains transformed with plasmids expressing full-length wild-type Sth1 or M4 mutant (L120A/V1206A/I1208A/L1210A) at different temperatures. (b) Spotting assays with *snf5Δ* strain transformed with plasmids expressing full-length wild-type Snf5 or M4 mutant (L785A/L787A/I789A/L791A) at different temperatures. (c) Spotting assays with *sth1Δ* strains transformed with plasmids expressing full-length wild-type Sth1 or M4 mutant on plates containing 20 mM hydroxyurea (HU), 0.015 % methyl methane sulfonate (MMS), and 10 mg/ml phleomycin (Phle) at 30 °C. (d) Spotting assays with *snf5Δ* strains transformed with plasmids expressing full-length wild-type Snf5 or M4 mutant on plates containing 20 mM hydroxyurea (HU), 0.015 % methyl methane sulfonate (MMS), and 10 mg/ml phleomycin (Phle) at 30 °C.